 

# Preparation and Characterization of a Microfabricated Oxide-on-Oxide Catalyst of $\alpha$-$Sb_2O_4$/$VSbO_4$

**Yusuke Ohminami,[1] Shushi Suzuki,[1] Nobuaki Matsudaira,[1] Tomoko Nomura,[2] Wang-Jae Chun,[1,2] Kaoru Ijima,[1] Motonori Nakamura,[3] Koichi Mukasa,[3] Masao Nagase,[4] and Kiyotaka Asakura*[,1]**

[1]Catalysis Research Center, Hokkaido University, Kita 21-10, Kita-ku, Sapporo 001-0021

[2]CREST of JST, Kita 21-10, Kita-ku, Sapporo 001-0021

[3]Nanoelectronic Laboratory, Graduate School of Engineering, Hokkaido University, Kita 13, Nishi 8, Sapporo 060-8628

[4]NTT Basic Research Laboratories, 3-1 Morinosato, Wakamiya, Atsugi, Kanagawa 243-0198

Received September 21, 2004; E-mail: askri@cat.hokudai.ac.jp

We have prepared microfabricated $\alpha$-$Sb_2O_4$ thin films on $VSbO_4$ by electron lithography. The $VSbO_4$ thin films were prepared on a Si substrate by a sol–gel method combined with a spin coating. The size, separation and arrangement of the $\alpha$-$Sb_2O_4$ overlayer were controlled by electron-beam lithography. We could successfully draw 0.5 μm wide lines with a separation of 2 μm. A preliminary study on the catalysis showed an enhancement of the selectivity in a propene conversion reaction to acrolein on a microfabricated $\alpha$-$Sb_2O_4$/$VSbO_4$.

Although catalytic reactions occur on an atomic-scale active site at surface, industrial catalysts contain two or more active structures, which communicate with each other through a diffusion of reactants in 10 nm to a few μm range. This communication determines the catalytic properties and enhances their performances. One may find examples in a remote-control catalyst, a phase-transfer catalyst and a spill-over catalyst.[1–3] The remote-control mechanism was originally proposed by Delmon, who intended to explain the selective oxidation of hydrocarbons on binary or ternary oxides.[2] The activation of stable hydrocarbons by oxygen and their selective conversion to useful organic compounds with less CO and $CO_2$ byproducts formation are a key issue for green chemistry. Many mixed oxides, such as V–P–O, Sn–Sb–O, V–Sb–O, Bi–Mo–O, and Pt/$SbO_x$, are examples for remote-control catalysts.[4–13] Gas-phase oxygen is activated on a so-called donor oxide phase, which has, in many cases, no or little activity of its own. The donor oxide phase supplies the oxygen to the other phase (an acceptor phase) through a spillover process, and continuously creates active and selective sites on the acceptor phase.[14,15] The migrated oxygen can reoxidize the other oxide phase much more easily or create a new active phase, such as Brönsted acid sites. If this concept is correct, we will have a new way to manage catalysis by adjusting the physical parameters, such as the size, shape, and arrangement of each phase in a nm–μm order or on a mezoscopic scale. However, it is not easy to adjust these physical parameters in the conventional catalysts, which are usually in a powder form.

One solution is to use a flat substrate. In the semiconductor industry, the electric circuits in devices such as CPU, memory and other LSI chips are drawn in a μm-nm size, using lithography methods. Recently, many attempts have been made to apply lithography methods to the production of microfabricated noble metal catalyst surfaces, where the size, shape, and arrangement are well-controlled.[16–36] Using these methods, one can reveal the dependence of catalyses on these parameters. In addition, we can characterize a microfabricated structure on a flat substrate surface by many surface science and microscopic techniques, such as scanning probe microscopy (SPM) and photoemission electron microscopy (PEEM), because of its flatness and no porosity.[17,18,37,38]

In spite of these pioneering studies, it is still difficult to prepare microfabricated oxide on another oxide surface by electron lithography, because electron lithography requires electric conductivity though many oxides are insulators. Previously, thin oxide films were developed on Si substrates for the substrates of the microfabricated metal domains created by lithography. However, they had no well-defined crystalline structures.[21–36] In this work we prepared a microfabricated $\alpha$-$Sb_2O_4$ crystalline film on crystalline $VSbO_4$ in their crystalline structures by lithography, where $\alpha$-$Sb_2O_4$ is the donor site for oxygen supply and the $VSbO_4$ is the acceptor phase. Because $VSbO_4$ substrate is an insulator, it is difficult to directly apply lithography on a $VSbO_4$ single crystal. We prepared a crystalline $VSbO_4$ thin film as a substrate, which was developed on a Si surface. We had to be careful to prepare the thin film oxide because phase separation may easily occur to $V_2O_5$ and $Sb_2O_4$, and there are several Sb–V–O phases, such as $SbV_2O_7$. Our first trial was to establish a preparation method of the microfabricated oxide on another oxide surface with well-defined crystal structures. The problems that we had to resolve are listed below:

1. The underlayer of $VSbO_4$ must be sufficiently flat to form the pattern by lithography.
2. The underlayer of $VSbO_4$ must have a well-defined crystal structure.
3. The underlayer of $VSbO_4$ must have an appropriate thickness to maintain the electron conductivity and good

Published on the web March 11, 2005; DOI 10.1246/bcsj.78.435

crystallinity.

4. The overlayer of $Sb_2O_4$ must have an $\alpha$-type crystalline structure, though several polymorphisms are present in the Sb oxides.

In this paper we report on the successful preparation of microfabricated $\alpha$-$Sb_2O_4$ on a $VSbO_4$ surface. As far as the authors know, this is the first example of preparing a microfabricated oxide film on another oxide with definite crystal structures. The reaction experiments on the microfabricated surface are another problem, due to its low surface area. In the final part we show preliminary results of catalyses of the fabricated $\alpha$-$Sb_2O_4/VSbO_4$. We found the first evidence that the microfabricated surface improved the catalytic properties.

## Experimental

**Reagents.** We used n-type Si(100) single crystals with a 100 nm naive $SiO_2$ film as substrate. It was soaked in a detergent, Semicoclean 23 (Furuuchi Chemical Co.), followed by supersonic cleaning. The sample was then rinsed with pure water. Reagent-grade $V_2O_5$ and $Sb_2O_3$ were purchased from Kanto Chemical Co. Reagent-grade $H_2O_2$ (Mitsubishi Gas cooperation) was used without a further purification.

**Preparation Procedure.** The preparation scheme is summarized in Fig. 1. We first prepared the $VSbO_4$ film. The sample was then covered with a resist, and exposed to an electron beam to draw resist patterns. The $\alpha$-$Sb_2O_4$ film was deposited and the resist was removed to form microfabricated $\alpha$-$Sb_2O_4/VSbO_4$.

A $VSbO_4$ film was deposited on a Si surface by a spin-coating method of a V–Sb–O sol solution. The V–Sb–O sol solution was prepared according to the literature.[39] $V_2O_5$ was suspended in an aqueous solution and reacted with $H_2O_2$. After a dark-red solution was obtained, a $Sb_2O_3$ suspension was added. The solution was refluxed and stirred for 4 h. The color finally turned black. The water was then evaporated until the viscosity of the solution reached 1.2 cP. The thus-obtained V–Sb–O sol solution was deposited onto the Si substrate by spin coating. A few mL of the sol solution was put at the center of a Si substrate, and the sample was rotated at 500 rpm for the first 10 s and 3000 rpm for the next 30 s using a spin coater (1H-D7, Mikasa Co.). The sample was dried at 393 K and further calcined in air at 773 K.

The lithography was carried out using an electron lithography instrument (Elionics ELS-3700). The sample was washed sequentially with dimethylformamide (DMF), acetone, and ethanol for 5 min, respectively. In each solvent, ultrasonic cleaning was applied to the sample. The resist (ZEP520) was then deposited on the sample by spin coating, followed by a heat treatment for 2 min at 453 K. The sample was exposed to an electron beam to draw resist patterns. The development of the resist patterns was made in a ZED-N50 solution for 5 min, which was rinsed with ZED-B for 20–30 s.

Deposition of the $\alpha$-$Sb_2O_4$ film was carried out by the vacuum evaporation of $Sb_2O_3$, followed by resist removal and oxidation at 673 K. The $Sb_2O_3$ powder was set on a W boat, which was resistively heated under $3 \times 10^{-3}$ Pa. The thickness was monitored by a quartz thickness monitor. The resist was removed off by dipping the sample sequentially in DMF, acetone and ethanol under ultrasonic power. After removing the resist, the sample was oxidized at 673 K.

An $\alpha$-$Sb_2O_4/Si$ sample was prepared for a comparison by the vacuum deposition of $Sb_2O_3$ onto the Si surface and calcined in air at 673 K. $VSbO_4/Si$ was also prepared by the spin-coating method of the $VSbO_4$ sol solution, followed by calcination at 773 K.

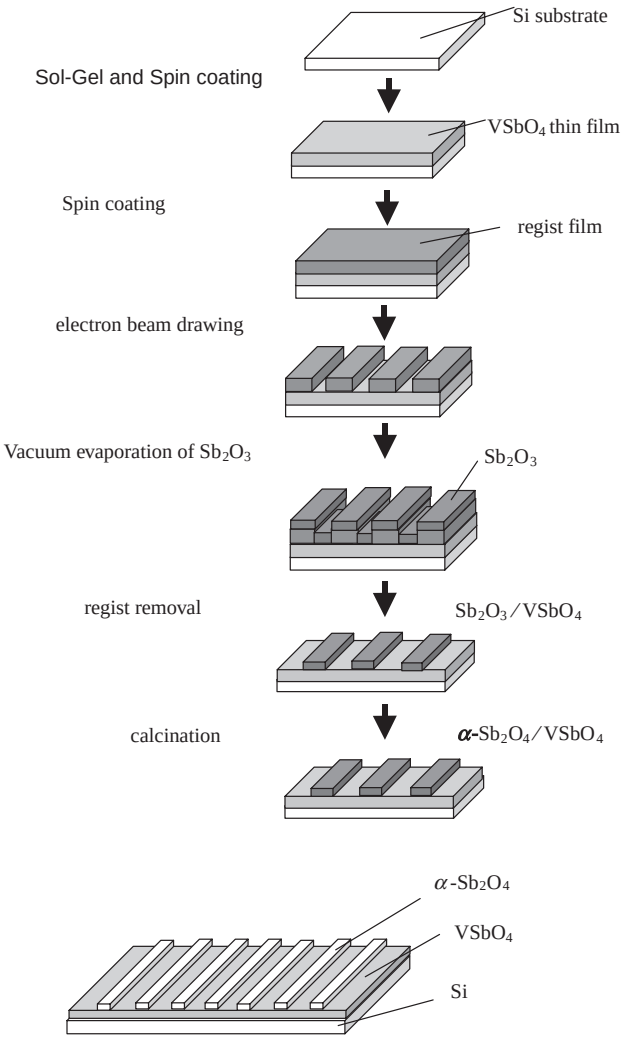


Fig. 1. Preparation scheme of the microfabricated $\alpha$-$Sb_2O_4/VSbO_4/Si$.

**Characterization.** In order to analyze the thin film structure, we used glancing-angle in-plane X-ray diffraction (RIGAKU RINT2500H using a Cu K$\alpha$ line). The surface composition was determined by XPS (Al K$\alpha$ Kratos XSAM800). The binding energy was calibrated by the C 1s peak, which was set at 285 eV. The morphology was given by AFM (Seiko Instrument, SPA500). A Si cantilever was used with its spring constant 40 N/m. Scanning electron microscopy and scanning Auger microscopy were performed with a Hitachi S-800.

**Catalytic Reactions.** The difficulty to evaluate catalyses in the fabricated oxides is that the electron lithograph can provide a small area of the fabricated surface in a reasonable timescale, which is $10^{-5}$–$10^{-6}$ times as small as that of the conventional powder catalyst.[34] In order to increase the detection sensitivity of the reaction products, a circulating reaction system or a static batch system is more preferable. However, in the oxidation reaction, a too-long residence time of the products induces a total combustion reaction to CO and $CO_2$. We chose a flow-reaction system. Therefore, a high detector sensitivity and less reactivity of the reactor wall, sample holders and heating materials are strongly required. Figure 2 shows the catalytic reaction system.

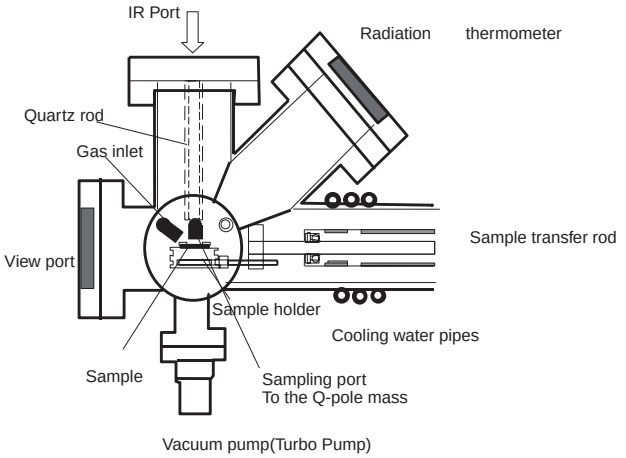


Fig. 2. A reaction chamber for the microstructured $\alpha$-$Sb_2O_4/VSbO_4/Si$.

The base pressure of the chamber was $10^{-5}$ Pa. In order to reduce the secondary reactions, the space above the sample was evacuated through a 1/16″ sampling tube, which was connected to a quadrupole mass spectrometer (Spectra Co. Micron Plus), as shown in Fig. 2. Because the sample surface area was very small, we had to be careful against contaminations of the sample. The sample was cleaned in high purity acetone and ethanol under ultrasonic power and oxidized by $3 \times 10^{-4}$ Pa oxygen at 673 K for 2 h. We used an infrared heating system (Thermo Riko Co., GVH198) to prevent heating other parts than the sample. Instead of using a resistive heater attached to the sample, only the sample could be heated locally by the infrared beam, and the reactions on a sample holder or heating materials were negligible. The infrared emitted from a W lamp outside the chamber was focused onto the sample through a quartz tube with a diameter of 1 $mm^{\phi}$. As a result, only the sample could be heated up to 1000 K. We cut the samples from the Si substrate to keep the exposed area of $VSbO_4$ to be constant because the $VSbO_4$ was the active site. Although the V–Sb–O catalyst is a propane ammoxidation catalyst, we carried out a preliminary reaction of propene oxidation on a microfabricated $Sb_2O_4$–$VSbO_4$ system, because the propene oxidation reaction occurs more easily. The total pressure was about $5.4 \times 10^{-1}$ Pa ($1.8 \times 10^{-1}$ Pa $O_2$ and $3.6 \times 10^{-1}$ Pa $C_3H_6$). The flow rate was $6 \times 10^{-9}$ mol/s. The reaction temperature was 540 K.

## Results and Discussion

**$VSbO_4$ Thin Layer Film Preparation.** There are several methods to construct a binary thin oxide film, such as CVD, MBE, laser aberration, electron-beam evaporation, and sputtering. We adopted sol–gel method with spin coating to obtain a single-phase $VSbO_4$. The sol–gel method has great advantages over the other methods, because: 1) It is simple and economical. 2) The composition can be controlled by the added amount of precursor materials. 3) It gives a flat and homogeneous film when the sol solution is deposited by an appropriate method.

We prepared the sol solution in the same way as reported for the preparation of V–Sb–O catalyst powder, which gave a $VSbO_4$ structure after calcinations at 773 K.[40] A homogeneous V–Sb–O gel film was deposited onto a Si substrate by two methods using the same sol solution, i.e., a dipping method and a spin-coating method. The dipping method was used to deposit the oxide sol solution onto Si substrate by dipping the Si substrate into the sol solution and pulling it out of the solution at a constant rate. The spin-coating method was used to disperse the oxide sol solution by rotating the Si substrate at high speed. Both methods could give a uniform and flat V–Sb–O film, but the spin-coating method was more reliable and reproducible. Thus, we mainly prepared the $VSbO_4$ film by the spin-coating method. The spin-coating method disperses catalytic precursors on a flat support homogeneously by the centrifugal force, which replaces the capillary force exerted in the impregnation processes of porous oxide materials, such as $SiO_2$ and $Al_2O_3$.[41–43] Gaigneaux et al. synthesized $\alpha$-$MoO_3$ thin films with good crystallinity and a controllable film thickness by the spin coating.[43]

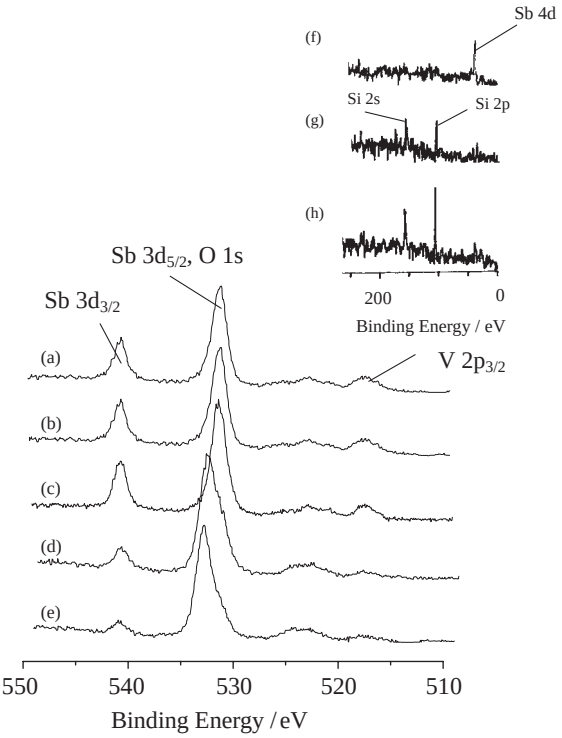


Fig. 3. X-ray photoelectron of $VSbO_4/Si$ calcined at 673 K (a), 773 K (b), 873 K (c), 973 K (d), and 1073 K (e). Upper inset gives the XPS in the Si 2s and 2p regions after the calcination at 873 K (f), 973 K (g), and 1073 K (h).

Figure 3 shows the X-ray photoelectron spectra for the V 2p, Sb 3d, and O 1s peaks. The Sb $3d_{5/2}$ peak appeared very close to the O 1s peak; we used the Sb $3d_{3/2}$ peak for further discussion. The binding energies of Sb $3d_{3/2}$ and V $2p_{3/2}$ for the samples calcined at 673 K, 773 K and 873 K were 540.8 eV and 517.5 eV, respectively. These values well corresponded to the reported binding energies in $VSbO_4$ (Sb $3d_{3/2}$ 540.9 eV and V $2p_{3/2}$ 517.5 eV).[44] The peak-area ratio of Sb $3d_{3/2}$ to V $2p_{3/2}$ was $2.4 \pm 0.3$, which well corresponded to the 1:1 ratio expected from the theoretical sensitivity factors (2.35).[44] The Sb $3d_{3/2}$ and V $2p_{3/2}$ peaks decreased at 973 K. The peak at 531.5 eV, corresponding to O 1s and Sb $3d_{5/2}$, was shifted to a higher binding energy (532.5 eV) because of a decrease in the contribution of Sb $3d_{5/2}$, which appeared at a lower binding energy than the O 1s peak. At the same temperature, the Si peak appeared as shown in the inset of Fig. 3(g). Thus, the

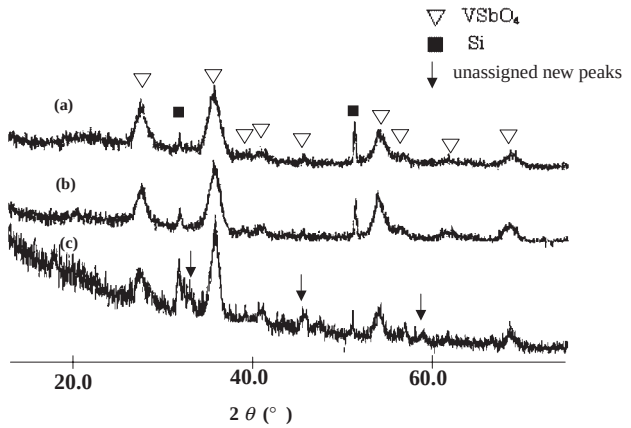


Fig. 4. X-ray diffraction of the $VSbO_4$/Si calcined at 673 K (a), 773 K (b), and 873 K (c).

$VSbO_4$ film structure was destroyed at 973 K.

Figure 4 shows the XRD patterns of the $VSbO_4$ thin film on a Si substrate after a calcinations at 673 K, 773 K, and 873 K. When the sample was calcined above 673 K, we found peaks at $2\theta = 27.3°$, 35.4°, and 53.6° characteristic to the (110), (101), and (211) peaks of $VSbO_4$, respectively. Smaller peaks appeared at 40°, 44°, 56.9°, 60°, and 68°, which were consistent with the (111), (210), (220), (002), and (301) diffraction peaks of $VSbO_4$. The last peak may be overlapped with (112) ($2\theta = 67.73°$). The peak width was slightly reduced after a calcination at 773 K ($\Delta(2\theta) = 1.2°$ (673 K) $\rightarrow$ 1.0° (773 K) for $2\theta = 27.3°$, $\Delta(2\theta) = 1.3°$ (673 K) $\rightarrow$ 1.2° (773 K) for 35.4°, $\Delta(2\theta) = 1.5°$ (673 K) $\rightarrow$ 1.0° (773 K) for 53.6°). The $VSbO_4$ crystalline structure was formed at 673 K and the 773 K calcination improved the crystallinity. However, at 873 K, new peaks appeared at 36°, 46°, and 59° (indicated by arrows in Fig. 4c), which could not be assigned to $VSbO_4$, indicating a partial destruction of the $VSbO_4$ structure. Thus, $VSbO_4$ film was calcined at 773 K for further processing. Figure 5a depicts the AFM picture for the $VSbO_4$ film calcined at 773 K. We found that the film was composed of 10–20 nm small particles, and that the average roughness of the surface was 20 nm. Figure 5b showed the SEM picture measured from the side of the substrate. The thickness of the $VSbO_4$ film was about 4.7 μm.

**$\alpha$-$Sb_2O_4$ Thin Layer Film Preparation on $VSbO_4$. Evaporation of $Sb_2O_3$:** We then deposited the $\alpha$-$Sb_2O_4$ thin film onto $VSbO_4$ that was precovered with a micro-patterned organic resist. Deposition of the $\alpha$-$Sb_2O_4$ had some problems. The spin coating of an Sb oxide sol solution was difficult because there was already organic resist materials on the $VSbO_4$ surface that would repel the sol aqueous solution and block the homogeneous deposition of the Sb oxide sol film. Another possible way was the vacuum deposition of metallic Sb. The complete oxidation of metallic Sb to form the $\alpha$-$Sb_2O_4$ required a temperature higher than 1000 K, which would damage the $VSbO_4$ film.[45] We used $Sb_2O_3$ vacuum evaporation because $Sb_2O_3$ had an appropriate vapor pressure at elevated temperatures, and pure $\alpha$-$Sb_2O_4$ crystal was usually obtained by the calcination of $Sb_2O_3$ in air.[9] First, we investigated the behavior of the $Sb_2O_3$ film on a bare $VSbO_4$ film during the calcination processes.

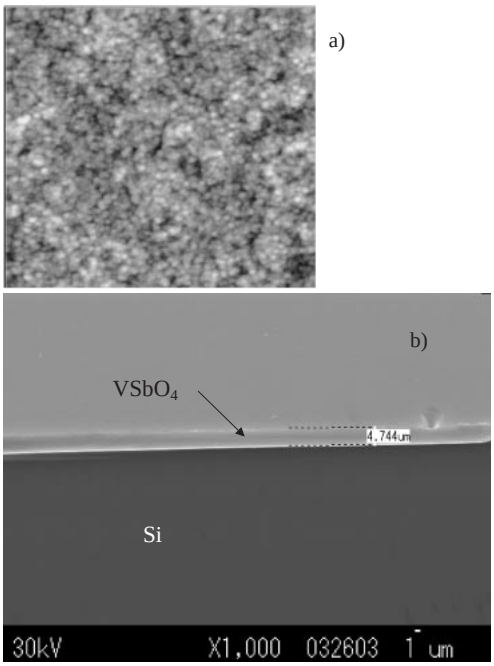


Fig. 5. A surface topography (a) and a side view (b) of $VSbO_4$/Si surface calcined at 773 K. (a) was measured by AFM and (b) was measured by SEM.

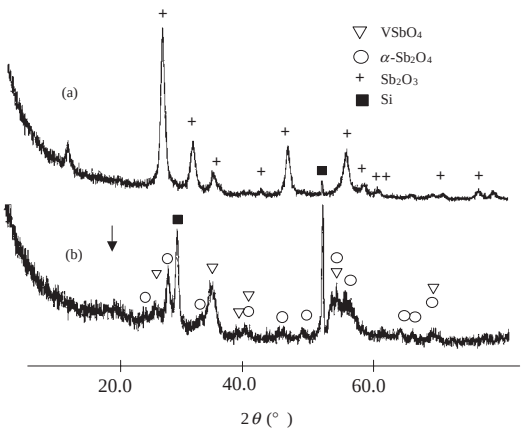


Fig. 6. X-ray diffraction of $Sb_2O_3$ deposited on the $VSbO_4$/Si calcined at 573 K (a) and 673 K (b).

**Calcination Conditions and the Structure of the Deposited $Sb_2O_3$ Thin Layer:** We deposited about 20 nm thick $Sb_2O_3$ on the $VSbO_4$/Si by vacuum evaporation. Figure 6 shows the XRD of the $Sb_2O_3$/$VSbO_4$/Si calcined at 573 K and 673 K. At 573 K, peaks appeared at 13.8°, 27.8°, 32.3°, 35.2°, 46.0°, and 54.5°, which corresponded to the (111), (222), (400), (331), (440), and (622) peaks of $Sb_2O_3$ (Senarmontite), respectively. After calcination at 673 K the peaks characteristic to $Sb_2O_3$ completely disappeared and these attributed to the $\alpha$-$Sb_2O_4$ peaks were present at 25.8°, 29.0°, 33.7°, 40.2°, 45.3°, 46.0°, 48.9°, 53.9°, 56.1°, 63.1°, 65.1°, and 68.3°. Thus the $\alpha$-$Sb_2O_4$ film could be obtained by calcinations at 673 K. Figure 7 shows the photoelectron spectra of the $\alpha$-$Sb_2O_4$ on the $VSbO_4$ after calcination at 673 K, 773 K, and 873 K. We only found a Sb peak at a calcination temper-

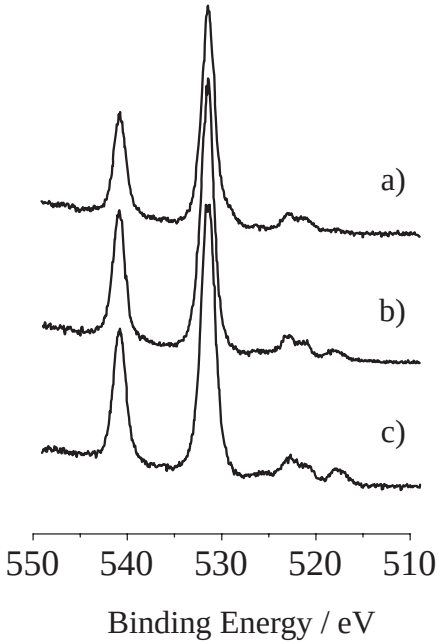


Fig. 7. X-ray photoelectron of the $Sb_2O_3/VSbO_4/Si$ calcined at 673 K (a), 773 K (b), and 873 K (c).

ature at 673 K, though the V peak appeared at 517.5 eV after calcination at 773 K. It was due to a breakdown of the $\alpha$-$Sb_2O_4$ overlayer. Thus, we calcined the $Sb_2O_3$ on $VSbO_4$ at 673 K.

**Lithography.** Our final goal was to prepare a fabricated $\alpha$-$Sb_2O_4$ surface on $VSbO_4$ by lithography, as shown in Fig. 1. We first doubted whether it would be possible to coat the $VSbO_4$ surface with the resist homogeneously, because the $VSbO_4$ film was composed of small particles with its average roughness of 20 nm, as shown in Fig. 5a. Second, we were afraid that the $VSbO_4$ thickness (4.7 μm) might be too large for electron lithography. However, the resist successfully wetted the $VSbO_4$ oxide surface. The electron beam could draw line pattern on a μm scale. On this resist pattern, $Sb_2O_3$ was deposited by vacuum evaporation with its thickness of 20 nm. The $Sb_2O_3$ patterns on the $VSbO_4$ were sometimes lost during the resist removal. This was due to the weak adhesion between $Sb_2O_3$ and $VSbO_4$ film, probably due to the presence of physisorbed $H_2O$ on the surface of $VSbO_4$. We deposited the $Sb_2O_3$ onto the $VSbO_4$ surface at 373 K under a high vacuum. Consequently, the $Sb_2O_3$ film was stably present after removal of the resist. Figure 8a shows an optical microscopic picture of the fabricated $Sb_2O_3$ pattern on the $VSbO_4$. Before calcination of the sample, 2 μm wide $Sb_2O_3$ lines were present on the $VSbO_4$ with a separation of 8 μm. Then, the microfabricated $Sb_2O_3$ on the $VSbO_4$ was calcined at 673 K to be converted to $\alpha$-$Sb_2O_4$ film. The fabricated structure was maintained after calcination at 673 K, as shown in Fig. 8b. Figure 9 shows an AFM image of the microfabricated $\alpha$-$Sb_2O_4$ on the $VSbO_4$. The thickness of the $\alpha$-$Sb_2O_4$ layer decreased to 7.0 nm due to a partial evaporation of $Sb_2O_3$, but the border between $\alpha$-$Sb_2O_4$ and $VSbO_4$ was clearly observed, indicating that little surface diffusion of the $\alpha$-$Sb_2O_4$ component to $VSbO_4$ surface occurred. The width of the border was less than a few tens of nm, judging from the AFM picture. These results indicated that

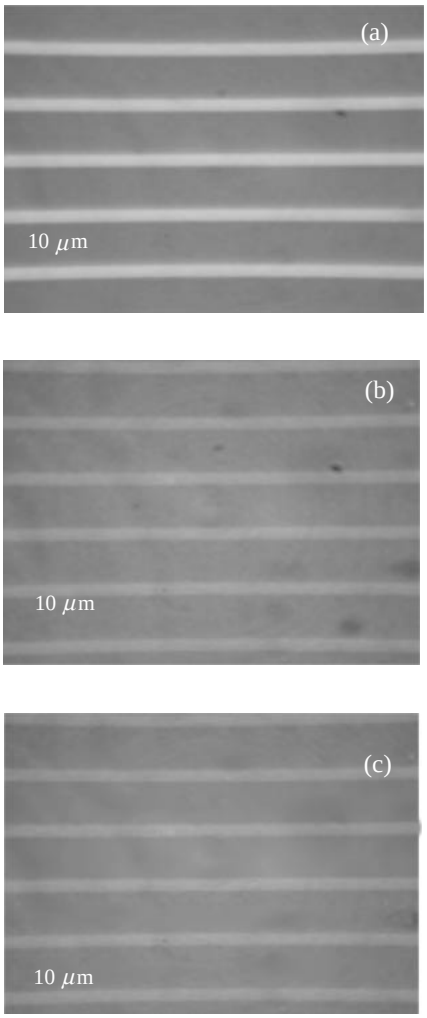


Fig. 8. Optical microscopic pictures of the fabricated $\alpha$-$Sb_2O_4/VSbO_4/Si$ by electron lithography; (a) before 673 K calcination; (b) after 673 K calcination; (c) after $Ar^+$ sputtering; (white part is $\alpha$-$Sb_2O_4$, black part is $VSbO_4$).

we could successfully perform electron lithography on a 4.7 μm thick $VSbO_4$ insulator film.

Figure 10 shows the selected-area Auger spectra of the $VSbO_4$ region on the fabricated surface. Before calcination we found both the V and Sb peaks in the $VSbO_4$ region. After calcination at 673 K, the V peak decreased and the Sb peak, increased indicating evaporation of the $Sb_2O_3$ and its re-deposition onto the bare $VSbO_4$ surface. In order to remove this thin Sb oxide overlayer on the $VSbO_4$, the microfabricated surface was treated by $Ar^+$ sputtering. The chamber was filled with $1 \times 10^{-5}$ Pa $Ar^+$ and the sample was sputtered with $Ar^+$ with an acceleration energy of 2.5 kV and an emission current of 25 mA for 20 min. Figure 9c shows the selected-area Auger spectra after the $Ar^+$ sputtering. The Sb oxide on the $VSbO_4$ region was removed and the V peak intensity of the $VSbO_4$ film was recovered to the original values. Figure 8c shows an optical microscopy picture after $Ar^+$ sputtering. The 2 μm width of the $\alpha$-$Sb_2O_4$ lines with 8 μm separation were maintained after $Ar^+$ sputtering.

Figure 11 shows the microfabricated $\alpha$-$Sb_2O_4$ patterns on

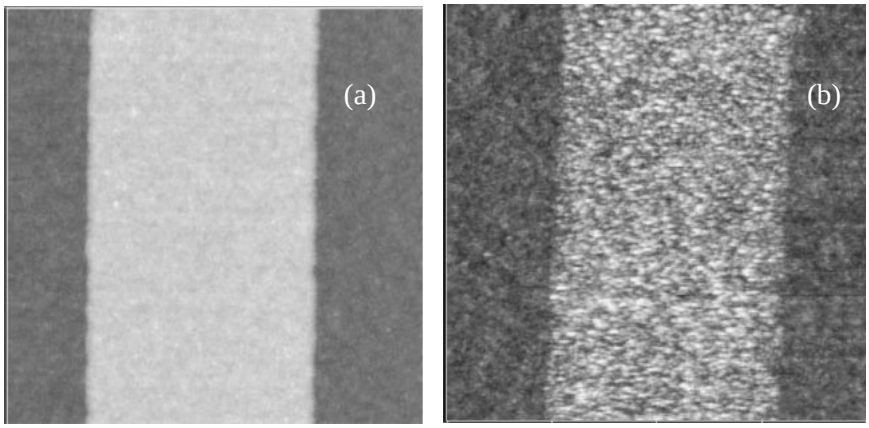


Fig. 9. AFM images of the microfabricated $\alpha$-$Sb_2O_4$/$VSbO_4$/Si; before 673 K calcination; (b) after 673 K calcination.

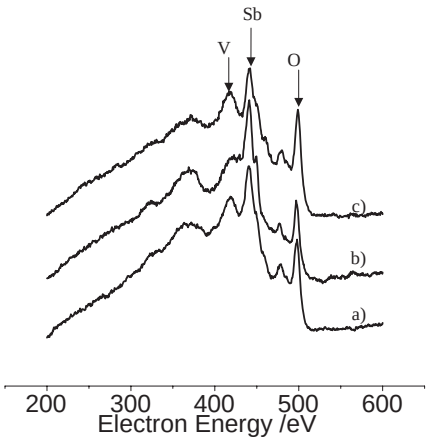


Fig. 10. Spot Auger spectra of fabricated $\alpha$-$Sb_2O_4$/$VSbO_4$/Si; (a) before 673 K calcination; (b) after 673 K calcination; (c) after $Ar^+$ sputtering.

$VSbO_4$ thin layers with different sizes and separations. At the moment we have succeeded to prepare the 0.5 μm $\alpha$-$Sb_2O_4$ lines with 2 μm separation. These microfabricated structures were stable against a calcination treatment at 673 K.

**Preliminary Results of Reactions.** We carried out propene oxidation reactions on the following three catalysts to evaluate the performance of the reaction instrument shown in Fig. 2 and to see the effect of the microfabricated structure on its catalysis: A $VSbO_4$/Si; B $\alpha$-$Sb_2O_4$/$VSbO_4$/Si; C $\alpha$-$Sb_2O_4$/Si.

The formation rates of acrolein and $CO_2$ converted from propene were followed by the quadrupole mass spectroscopy, as shown in Fig. 12. We could not find acrolein formation on the $\alpha$-$Sb_2O_4$ film, indicating that the background reaction on parts other than the sample was negligible. On the other hand, $VSbO_4$ bare surface showed the highest activities among the three. The rate was $(2.2 \pm 0.5) \times 10^{-11}$ mol $s^{-1}$ $cm^{-2}$. However, the main product was $CO_2$, and acrolein was formed with small selectivity (28%). When the $VSbO_4$ film was partially covered with $\alpha$-$Sb_2O_4$ ($\alpha$-$Sb_2O_4$ width = 2 μm, separation = 8 μm), the formation rate of acrolein was $(1.1 \pm 0.4) \times 10^{-11}$ mol $s^{-1}$ $cm^{-2}$ with a higher selectivity toward acrolein (nearly 60%) than that of the fully $VSbO_4$-exposed surface.

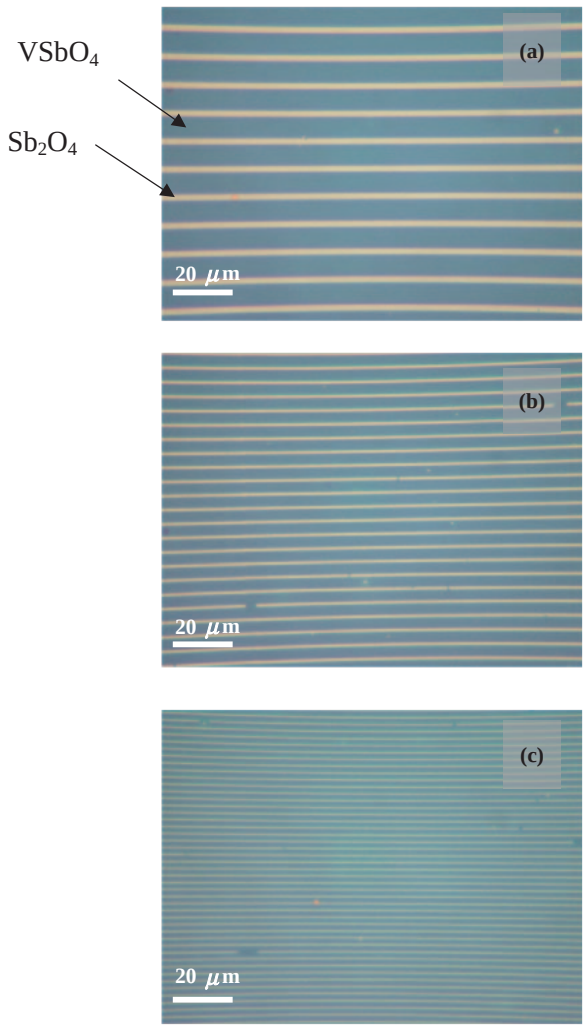


Fig. 11. Optical microscopy of the microfabricated $\alpha$-$Sb_2O_4$/$VSbO_4$/Si with different separations. (a) $\alpha$-$Sb_2O_4$ 2 μm, with 8 μm separation; (b) $\alpha$-$Sb_2O_4$ 1 μm, with 4 μm separation; (c) $\alpha$-$Sb_2O_4$ 0.5 μm, with 2 μm separation.

Although further studies to optimize the reaction conditions must be necessary, still the microfabricated oxide-on-oxide surface can improve the catalytic performance.

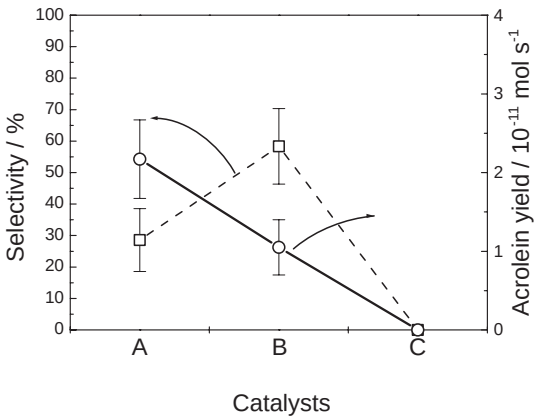


Fig. 12. Propylene oxidation reaction on (A) $VSbO_4/Si$, (B) microfabricated $\alpha$-$Sb_2O_4/VSbO_4/Si$. $\alpha$-$Sb_2O_4$ width is 2 μm, with 8 μm separation, and (C) $\alpha$-$Sb_2O_4/Si$. Open squares and open circles correspond to the selectivity and the yield of acrolein formation, respectively.

## Summary and Conclusion

1) We first prepared a well-defined microfabricated oxide-on-oxide surface in order to control the inhomogeneity of the surface by electron lithography by applying the following strategies:
   a) The use of Si as a substrate, which is flat enough and has a high electric conductivity appropriate for electron lithography.
   b) A crystalline $VSbO_4$ thin film with a sufficient flatness can be obtained by the sol–gel method and a spin-coating technique.
   c) The $\alpha$-$Sb_2O_4$ overlayer is prepared by the vacuum evaporation of $Sb_2O_3$, followed by the calcination at 673 K.
2) Electron lithography can control the size and separation of the microfabricated oxide film down to 0.5 μm at present.
3) The microfabricated oxide-on-oxide catalyst can improve the selectivity for partial oxidation reactions.
4) The microfabricated oxide-on-oxide will open a new way to investigate a heterogeneous catalyst, and to control its catalyst inhomogeneity.

The work has been supported by the CREST program and a Joint program between University and Industry, "EXPEEM," of JST and Exploratory Research program of Grants-in-Aid for Scientific Research of Ministry of Education, Culture, Sports, Science and Technology, No 14654127 (2002–2003). We give thanks to Rigaku Co. for XRD measurements.

## References

1 "New Aspects of Spillover Effect in Catalysis: Foe Development of Highly Active Catalysts," ed by T. Inui, K. Fujimoto, T. Uchijima, and M. Masai, Elsevier, Amsterdam (1993).

2 E. V. Dehmlow and S. S. Dehmlow, "Phase Transfer Catalysis," VCH, Weinheim (1993).

3 B. Delmon and G. F. Froment, *Catal. Rev.*, **38**, 69 (1996).

4 "Handbook of Heterogeneous Catalysis," ed by G. Ertl and H. Knozinger, VCH, Weinheim (1997).

5 W. Ueda, K. Oshihara, D. Vitry, T. Hisano, and Y. Kayashima, *Catal. Surv. Asia*, **6**, 33 (2002).

6 T. Inoue, K. Asakura, W. Li, S. T. Oyama, and Y. Iwasawa, *Appl. Catal.*, **165**, 183 (1997).

7 D. Carson, G. Coudurier, M. Forissier, J. C. Vendrine, A. Laarif, and F. Theobald, *J. Chem. Soc., Faraday Trans. 1*, **79**, 1921 (1983).

8 L. T. Weng, E. Sham, B. Doumain, P. Ruiz, and B. Delmon, "New Development in Selective Oxidation," ed by G. Centi and F. Trifiro, Elsevier, Amsterdam (1990), p. 757.

9 L. T. Weng, K. N. Spitaels, B. Yasse, J. Ladriere, P. Ruiz, and B. Delmon, *J. Catal.*, **132**, 319 (1991).

10 Y. Moro-oka and W. Ueda, *Adv. Catal.*, **40**, 233 (1994).

11 B. Zhou, E. Sham, T. Machej, P. Bertrand, P. Ruiz, and B. Delmon, *J. Catal.*, **132**, 157 (1991).

12 E. M. Gaigneaux and P. R. B. Delmon, *Catal. Today*, **32**, 37 (1996).

13 E. M. Gaigneaux, P. Ruiz, E. E. Wolf, and B. Delmon, *Appl. Surf. Sci.*, **121/122**, 552 (1997).

14 B. Delmon and G. F. Froment, *Catal. Rev.*, **38**, 69 (1996).

15 L. Weng, P. Ruiz, and B. Delmon, "New Developments in Selective Oxidation by Heterogeneous Catalysis," ed by P. Ruiz and B. Delmon, Elsevier, Amsterdam (1992), pp. 399–413.

16 I. Zuburtikudisand and H. Saltsburg, *Science*, **258**, 1337 (1992).

17 M. D. Graham, Y. G. Kevrekidis, K. Asakura, J. Lauterbach, H. H. Rotermund, and G. Ertl, *Science*, **264**, 80 (1994).

18 M. D. Graham, M. Baer, I. G. Kevrekidis, K. Asakura, J. Lauterbach, H. H. Rotermund, and G. Ertl, *Phys. Rev. E*, **52**, 76 (1995).

19 J. Lauterbach, K. Asakura, P. B. Rasmussen, H. H. Rotermund, M. Baer, M. D. Graham, I. G. Kevrekidis, and G. Ertl, *Physica D*, **123**, 493 (1998).

20 F. Esch, S. Günther, E. Schutz, A. Schaak, I. G. Kevrekidis, M. Marsi, M. Kiskinova, and R. Imbihl, *Surf. Sci.*, **443**, 245 (1999).

21 S. Y. Shvartsman, E. Schutz, R. Imbihl, and I. G. Kevrekidis, *Catal. Today*, **70**, 301 (2001).

22 E. Schutz, N. Hartmann, Y. Kevrekidis, and R. Imbihl, *Faraday Discuss.*, **105**, 47 (1996).

23 M. Pollmann, H. H. Rotermund, G. Ertl, X. J. Li, and I. G. Kevrekidis, *Phys. Rev. Lett.*, **86**, 6038 (2001).

24 X. Su, J. Jensen, M. X. Yang, M. B. Salmeron, Y. R. Shenand, and G. A. Somorjai, *Faraday Discuss.*, **105**, 263 (1996).

25 M. X. Yang, P. W. Jacobs, C. Yoon, L. Muray, E. Anderson, D. Attwoodand, and G. A. Somorjai, *Catal. Lett.*, **45**, 5 (1997).

26 A. S. Eppler, G. Rupprechter, L. Guczi, and G. A. Somorjai, *J. Phys. Chem. B*, **101**, 9973 (1997).

27 P. W. Jacobs, F. H. Ribeiro, and G. A. Somorjai, *Catal. Lett.*, **37**, 131 (1996).

28 J. Grunes, J. Zhu, E. A. Anderson, and G. A. Somorjai, *J. Phys. Chem. B*, **106**, 11463 (2002).

29 S. Johansson, K. Wong, V. P. Zhdanov, and B. Kasemo, *J. Vac. Sci. Technol., A*, **17**, 297 (1999).

30 A. C. Krauth, K. H. Lee, G. H. Bernstein, and E. E. Wolf, *Catal. Lett.*, **27**, 43 (1994).

31 A. C. Krauth, G. H. Bernstein, and E. E. Wolf, *Catal. Lett.*, **45**, 177 (1997).

32 S. Johansson, L. Osterlund, and B. Kasemo, *J. Catal.*, **201**,

275 (2001).
33 S. Johansson, E. Fridell, and B. Kasemo, *J. Vac. Sci. Technol., A*, **18**, 1514 (2000).
34 S. Johansson, E. Fridell, and B. Kasemo, *J. Catal.*, **200**, 370 (2001).
35 B. Kasemo, S. Johansson, H. Persson, P. Thormahlen, and V. P. Zhdanov, *Top. Catal.*, **13**, 43 (2000).
36 B. Kasemo, *Surf. Sci.*, **500**, 656 (2002).
37 S. Takakusagi, M. Kato, Y. Sakai, K. Fukui, K. Asakura, and Y. Iwasawa, *J. Microsc.*, **200**, 240 (2000).
38 H. Yasufuku, Y. Ohminami, T. Tsutsumi, K. Asakura, M. Kato, Y. Sakai, Y. Kitajima, and Y. Iwasawa, *Chem. Lett.*, **2002**, 842.
39 M. A. Toft, J. F. Brazdil, Jr., and L. C. Glaeser, U. S. Patent 4784979 (1988).
40 M. A. Toft, J. F. Brazdil, Jr., and L. C. Glaeser, U. S. Patent 4879264 (1988).
41 E. W. Kuipers, C. Laszolo, and W. Wieldraaijer, *Catal. Lett.*, **17**, 71 (1993).
42 R. M. van Hardeveld, P. L. J. Gunter, L. J. van IJzendoorn, W. Wieldraaijer, E. W. Kuipers, and J. Niemantsverdriet, *Appl. Surf. Sci.*, **84**, 339 (1995).
43 E. M. Gaigneaux, K. Fukui, and Y. Iwasawa, *Thin Solid Films*, **374**, 49 (2000).
44 R. Nilsson, T. Lindblad, and A. Andersson, *J. Catal.*, **148**, 501 (1994).
45 S. E. Golunskiand and D. Jackson, *Appl. Catal.*, **48**, 123 (1989).